Pattern Formation in Force-free Magnetic Fields and Beltrami Flows

Feng Qing-Zeng

Department of Mechanics, Peking University, Beijing, 100871, China

Z. Naturforsch. **51a**, 1161–1169 (1996); received September 5, 1996

Force-free magnetic fields and Beltrami flows, which are selenoidal vector fields and satisfy the condition that the field vector is everywhere parallel to its curl, have complex topological structures and usually show chaotic behavior. The lines of force are determined by the equations of a 3-D (dimensional) dynamical system. In the integrable case, all lines of force lie on some families of tori. If the integrable solution undergoes a small perturbation, most of the original tori still exist but undergo a slight distortion (KAM tori). Near the original heteroclinic cycles emerges a chaotic layer. By superposition of the basic solutions of force-free magnetic fields one can get very complicated pictures: a single line of force could be space filling within some subspace of a 3-D region, which has a fractional dimension and a positive Lyapunov exponent, i.e. one gets a chaotic line of force or a fractal. At the same time there are still ordered regions in the chaotic surroundings. Tubes of force which are tangled or self-knotted embed in the chaotic sea. The KAM tori can also be disrupted through resonances, leading to increased chaotic regions. Thus, the effect of nonlinear dynamics plays an important role in the pattern formation of force-free magnetic fields and Beltrami flows.

1. Force-free Magnetic Fields and Beltrami Flows

Cosmic magnetic fields which occur in regions of high electrical conductivity and low density might often satisfy the force-free condition

$$\operatorname{curl} \boldsymbol{H} = \alpha \boldsymbol{H}, \tag{1}$$

where $\boldsymbol{H}$ denotes the intensity of the magnetic field, and α the scalar function of position, since the pressure gradients or gravitational or inertial forces cannot balance a Lorentz force in this situation [1]. Under this condition the current is everywhere parallel to the magnetic field, and the Lorentz force

$$\boldsymbol{L} = \frac{1}{4\pi} \operatorname{curl} \boldsymbol{H} \times \boldsymbol{H}$$

vanishes. Since

$$\operatorname{div} \boldsymbol{H} = 0 \tag{2}$$

we obtain

$$\boldsymbol{H} \cdot \operatorname{grad} \alpha = 0, \tag{3}$$

which follows from taking the divergence of (1). Therefore, the lines of force of a magnetic field always lie on surfaces of constant α; except in some region D

$$\alpha = \text{constant}, \tag{4}$$

then a single line of force may be space filling within some subspace of D, that is to say, there may be chaotic lines of force.

Woltjer [2] has proved that in a perfectly conducting fluid the magnetic helicity

$$\mathcal{H}_m = \int_v \boldsymbol{A} \cdot \operatorname{curl} \boldsymbol{A} \, \mathrm{d}v, \tag{5}$$

where the vector potential A is invariant, provided $\boldsymbol{n} \cdot \operatorname{curl} \boldsymbol{A} = 0$ on the surface S enclosing the volume V. Such a quantity represents the degree of linkage, or knottedness of the lines of force [3].

The motion of an incompressible inviscid fluid is described by the Euler equation

$$\frac{\partial \boldsymbol{u}}{\partial t} = \boldsymbol{u} \times \operatorname{curl} \boldsymbol{u} - \operatorname{grad} h, \tag{6}$$

where $h = p/\varrho + u^2/2$, and the continuity equation

$$\operatorname{div} \boldsymbol{u} = 0. \tag{7}$$

Arnold [4] noticed that, since steady Euler flows satisfy

$$\boldsymbol{u} \cdot \operatorname{grad} h = 0, \tag{8}$$

the streamlines generally lie on surfaces of constant h, and the only situation which permits streamlines to escape this constraint occurs when the velocity vector is parallel to the vorticity vector everywhere in some region D, i.e.

$$\operatorname{curl} \boldsymbol{u} = \lambda \boldsymbol{u}. \tag{9}$$

Reprint requests to Prof. Feng Qing-Zeng.

0932-0784 / 96 / 1200-1161 $ 06.00 © – Verlag der Zeitschrift für Naturforschung, D-72072 Tübingen

This is a Beltrami flow, which poses actually the same mathematical problem as a force-free magnetic field. The streamlines of a Beltrami flow might be chaotic in regions where λ is constant. The corresponding phenomenon is called "Lagrangian turbulence" [5].

Moffatt [3] has proved that the flow helicity

$$\mathscr{H}_f = \int_v \boldsymbol{u} \cdot \operatorname{curl} \boldsymbol{u} \, dv \tag{10}$$

for a barotropic inviscid flow is invariant if $\boldsymbol{n} \cdot \operatorname{curl} \boldsymbol{u} = 0$ on the surface S which encloses the Volume V and moves with the fluid. This result might be interpreted in terms of conservation of linkage or knottedness of vortex lines. According to (9) a Beltrami flow has maximal helicity, which implies that there exist complex topological structures.

It may be important to note that a Beltrami flow can induce a steady force-free magnetic field in a perfectly conducting fluid, since we have

$$\frac{\partial H}{\partial t} = \operatorname{curl}(\boldsymbol{u} \times \boldsymbol{H}) = 0 , \tag{11}$$

provided $\boldsymbol{H}$ is parallel to $\boldsymbol{u}$ everywhere, and a force-free magnetic field cannot affect the motions. According to Woltjer's theorem, the force-free field with constant α represents the lowest state of magnetic energy that a closed system may attain. It proves in a general way the stability of force-free fields with constant α.

2. Solutions in Spherical Polar Coordinates

A force-free magnetic field can be expressed as the sum of two vector fields in the form

$$\boldsymbol{H} = \boldsymbol{T} + \boldsymbol{P} , \tag{12}$$

where $\boldsymbol{T}$ and $\boldsymbol{P}$ satisfy the equations

$$\operatorname{curl} \boldsymbol{T} = \alpha \boldsymbol{P} , \tag{13}$$

$$\operatorname{curl} \boldsymbol{P} = \alpha \boldsymbol{T} . \tag{14}$$

Obviously $\boldsymbol{T}$, $\boldsymbol{P}$, and $\boldsymbol{H}$ are solenoidal vector fields, and $\boldsymbol{H}$ satisfies (1). If we let

$$\boldsymbol{T} = \operatorname{grad} f \times \boldsymbol{r} , \tag{15}$$

where f is a scalar function, from (13) we have

$$\boldsymbol{P} = \frac{1}{\alpha} \operatorname{curl}(\operatorname{grad} f \times \boldsymbol{r}) . \tag{16}$$

$\boldsymbol{T}$ is called toroidal vector field, and $\boldsymbol{P}$ poloidal vector field. It was first suggested by Chandrasekhar [6] that a force-free field could have such a decomposition.

Since the left hand side of (14) can be expressed as

$$\operatorname{curl} \boldsymbol{P} = -\frac{1}{\alpha} \Delta(\operatorname{grad} f \times \boldsymbol{r}) = -\frac{1}{\alpha} \operatorname{grad}(\Delta f) \times \boldsymbol{r} ,$$

where Δ is the Laplacian, from (14) and (15) we have

$$\operatorname{grad}(\Delta f + \alpha^2 f) \times \boldsymbol{r} = 0 . \tag{17}$$

This condition requires

$$\Delta f + \alpha^2 f = g(\boldsymbol{r}) , \tag{18}$$

where g is an arbitrary scalar function of r. The solution of (18) can be expressed as the sum of two parts:

$$f = \psi(r, \theta, \varphi) + f_0(r) , \tag{19}$$

where ψ is the general solution of the Helmholtz equation

$$\Delta \psi + \alpha^2 \psi = 0 , \tag{20}$$

and f_0 is a special solution of (18). Since grad $f_0 \times \boldsymbol{r} = 0$, from (15) it is evident that f_0 has no physical consequence. We may therefore assume without loss of generality that

$$f_0 = 0 . \tag{21}$$

Separable solutions of equation (20) are easily obtained [7] and can be expressed in the form

$$\psi = R_\ell(\alpha r) \, Y_{\ell m}(\theta, \varphi) , \tag{22}$$

where R_ℓ is a general spherical function of order ℓ and represents an arbitrary linear combination of the spherical Bessel functions j_ℓ (first kind) and y_ℓ (second kind):

$$R_\ell(\alpha r) = A j_\ell(\alpha r) + B y_\ell(\alpha r) ; \tag{23}$$

and $Y_{\ell m}$ is a spherical harmonic function

$$Y_{\ell m}(\theta, \varphi) = C P_\ell^m(\cos\theta) \begin{Bmatrix} \cos m\varphi \\ \sin m\varphi \end{Bmatrix} , \tag{24}$$

where P_ℓ^m denotes the associated Legendre function, and (r, θ, φ) are spherical polar coordinates. With the function ψ given by (22), we can calculate $\boldsymbol{T}$ and $\boldsymbol{P}$, and the components of force-free magnetic fields in spherical polar coordinates can be written in the form

$$H_r = \ell(\ell+1) \frac{1}{\alpha r} R_\ell(\alpha r) \, Y_{\ell m}(\theta, \varphi) ,$$

$$H_\theta = R_\ell(\alpha r) \frac{1}{\sin\theta} \frac{\partial}{\partial \varphi} Y_{\ell m}(\theta, \varphi) + \frac{1}{\alpha r} \frac{\partial}{\partial r} [r R_\ell(\alpha r)] \frac{\partial}{\partial \theta} Y_{\ell m}(\theta, \varphi) ,$$

$$H_\varphi = -R_\ell(\alpha r)\frac{\partial}{\partial\theta}Y_{\ell m}(\theta,\varphi) + \frac{1}{\alpha r}\frac{\partial}{\partial r}[r R_\ell(\alpha r)]\frac{1}{\sin\theta}\frac{\partial}{\partial\varphi}Y_{\ell m}(\theta,\varphi), \quad (25)$$

$$\ell = 1, 2, 3, \ldots; \quad m = 0, 1, \ldots, \ell .$$

The case $m = 0$ corresponds to the axisymmetric field, which was given by Chandrasekhar [6].

The conditions at an interface where α changes discontinuously are

$$H_r = 0, \quad \text{and} \quad H_\theta \quad \text{and} \quad H_\varphi \text{ are continuous}. \quad (26)$$

The lines of force are determined by the equations

$$\frac{dr}{H_r} = \frac{r\,d\theta}{H_\theta} = \frac{r\sin\theta\,d\varphi}{H_\varphi}. \quad (27)$$

For the case $m = 0$, one integral can be obtained from the first two equations

$$r R_\ell(\alpha r)\sin\theta\, P_\ell^1(\cos\theta) = \text{constant}. \quad (28)$$

Therefore, the lines of force corresponding to the case $m = 0$ always lie on a 2-dimensional surfaces.

Consider now the force-free magnetic fields in a sphere, setting $B = 0$ in (23) to obtain bounded physical quantities, and setting $\alpha = 1$ (not losing generality).

3. Singular Points of the Vector Fields

Zero points of the intensity of the magnetic field are the singular points of the vector field where the direction of the field is indefinite. The intensity gradient matrix at the singular point is symmetrical, since its antisymmetrical part is related to the curl of the intensity of the force-free magnetic field which also vanishes at the singular point and has a zero trace as a result of a divergenceless the vector field. So its three eigenvalues are all real, the sum of which vanishes. Therefore, the singular points of a force-free magnetic field are generally hyperbolic. Except for the degenerate cases, either there are two negative eigenvalues or there are two positive eigenvalues. We shall call the former class type α singular points, and the latter type β (Domber et al. [3]).

Since we have $j_\ell(r) \sim r^\ell$ as r is small, the center of the sphere is always a singular point, except in the case $\ell = 1$. Other singular points of a single solution in (25) all lie on the spherical surfaces. The line of force joining two hyperbolic points is called heteroclinic line.

If we confine our attention to flows on the spherical surface, the sum of the Poincaré indices for all singularities on the sphere must equal 2 [8]. This number is called the Euler characteristic and is an important topological invariant. The Poincaré index of a curve in a plane vector field is the number of rotations of the field vectors along the curve. If the curve goes around a single center, focus or node, then the Poincaré index $I = +1$; whereas if it goes around a saddle $I = -1$. This number only depends on the nature of the singularity and is called an index of a singular point. The concept of Poincaré index can be generalized to the vector field on a sphere or other 2-D manifolds.

In the case $m = 0$, the north and south pole are nodes on the sphere, and there are $\ell - 1$ circles, paralleling the equator, which are made up of singular points on the sphere; the origin is a degenerate singular point for $\ell > 2$ (see Figure 1).

In the case $\ell = 3$, $m = 3$, the z-axis is a continuous set of singular points, and the north pole and south pole are 2-D saddles with three separatrices on the sphere (see Figure 2a). The Poincaré index of such a saddle equals -2. Figure 3 shows that the north pole saddle breaks up under a small 2-D perturbation (taking the solution $\ell = 3$, $m = 0$ as a perturbation term), forming three separate ordinary saddles, and a node (or a focus under more general 2-D perturbations [9]).

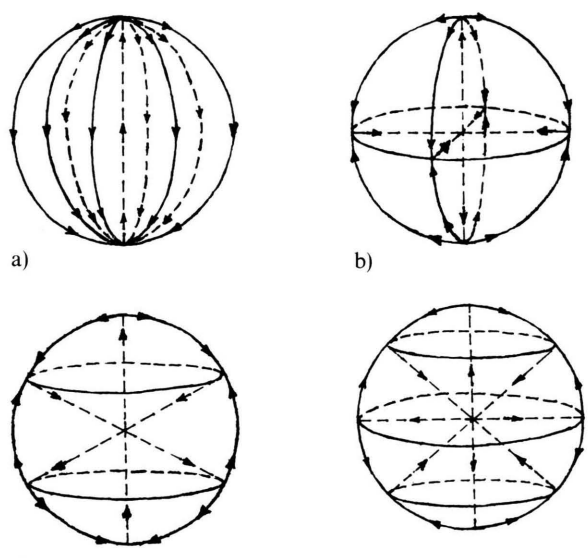

Fig. 1. Singular points and heteroclinic lines corresponding to the case $m = 0$.
a) $\ell = 1$; b) $\ell = 2$; c) $\ell = 3$; d) $\ell = 4$.

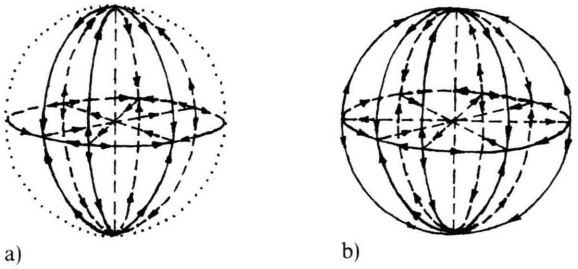

a) b)

Fig. 2. Singular points and heteroclinic lines corresponding to the case $\ell = m$.
a) $\ell = m = 3$; b) $\ell = m = 4$.

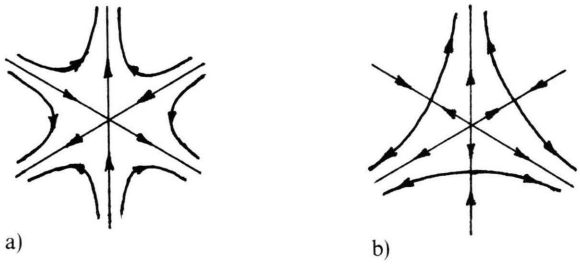

a) b)

Fig. 3. Structural instability of a degenerate saddle in the case $\ell = 3$, $m = 3$.
a) North pole saddle with three separatrices.
b) Such a saddle breaks up under a small 2-D perturbation, forming three separate ordinary saddles and a node.

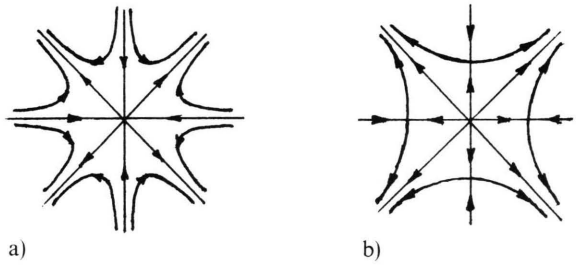

a) b)

Fig. 4. Structural instability of a degenerate saddle in the case $\ell = 4$, $m = 4$.
a) North pole saddle with four separatrices.
b) Such a saddle breaks up under a small 2-D perturbation, forming four separate ordinary saddles and a node.

There are six nodes on the equator, the three of which are stable and others unstable. The sum of the Poincaré indices for all singularities on the sphere is: $1 \times 6 - 2 \times 2 = 2$.

Similarly, in the case $\ell = 4$, $m = 4$, the north pole and south pole are 2-D saddles with four separatrices (see Fig. 2b), the Poincaré index of which equals -3. In Fig. 4, taking the solution $\ell = 4$, $m = 0$, as a perturbation term, such a saddle breaks up, forming four separate ordinary saddles and a node. There are eight nodes on the equator, four of which are stable and the others unstable. The sum of the Poincaré indices is $1 \times 8 - 3 \times 2 = 2$.

One can infer that in the case $\ell = n$, $m = n$, the north pole and south pole are 2-D saddles with n separatrices on the sphere, the Poincaré index of which equals $-n + 1$, and such a saddle can break up under small 2-D perturbations, forming n separate ordinary saddles, and a node (or a focus).

The concept of Poincaré index of a curve in a plane vector field can be generalized to higher dimension. We introduce rotation degree of a $(n-1)$-D closed hypersurface in a n-D vector field [10]. Let S denote a $(n-1)$-D closed hypersurface which has the local coordinates $X_1, X_2, \ldots, X_{n-1}$; and the n-D vector field $\boldsymbol{H}$ has no singular points on S, then the rotation degree of a vector field on S is

$$J = \frac{\Gamma\left(\frac{n}{2}\right)}{2\pi^{n/2}} \int_S \frac{1}{\| \boldsymbol{H} \|^n} \det\left(H, \frac{\partial H}{\partial X_1}, \ldots, \frac{\partial \boldsymbol{H}}{\partial X_{n-1}}\right) \cdot \mathrm{d}X_1 \wedge \ldots \wedge \mathrm{d}X_{n-1}, \tag{29}$$

where $\Gamma(\cdot)$ is a Gamma function, $\| \cdot \|$ Euclidean norm. If there is no singular point of the vector field in space encircled by S, then the rotation degree is zero; if there is an isolated singular point, then the rotation degree depends only on the nature of the singular point, and is irrelevant to the S, so it is called a rotation degree of a singular point.

In a 3-D vector field, the rotation degree of a saddle with 2-D stable manifold and 1-D unstable manifold (α singular point) is $+1$; the rotation degree of a saddle with 2-D unstable manifold and 1-D stable manifold (β singular point) is -1; and $J = 1$ for an unstable node; $J = -1$ for a stable node.

We calculate the rotation degree of the origin (center of the sphere) in the case $\ell = 3$, $m = 0$. The calculation results in $J = 0$ for this degenerate 3-D saddle, which has a 2-D stable manifold, a 2-D unstable manifold, an additional 1-D stable manifold, and an additional 1-D unstable manifold (see Figure 1c). The invariant manifolds of such a saddle can be simply obtained by rotating a 2-D saddle with three separatrices around one of the separatrices.

The rotation degree of the origin in the case $\ell = 4$, $m = 0$ is $+1$ or -1 (depending the sign of the constant C in (24)). The invariant manifolds of this degen-

erate 3-D saddle can be obtained by rotating a 2-D saddle with four separatrices around one of the separatrices (see Figure 1 d).

Generally speaking, the center of the sphere in the case $\ell = n$, $m = 0$, is a degenerate 3-D saddle as $n > 2$, the rotation degree of which is 0 as n is odd, or ± 1 as n is even. The author conjectures that such a degenerate 3-D saddle can break up under small perturbations, forming ordinary α saddles ($J = +1$) and β saddles ($J = -1$), and if n is odd, the number of α saddles equals the number of β saddles; if n is even, there will be one more α or β saddle.

Such high degenerate 2-D and 3-D singular points of the vector fields probably have not been seen before. It is very interesting from a point view of the dynamical system theory.

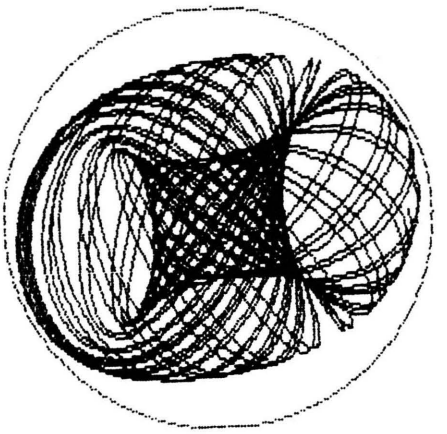

Fig. 5. A torus corresponding to the case $\ell = 1$.

4. 3-D Dynamical System and Configuration of the Lines of Force

The lines of force of a force-free magnetic field are determined by a 3-D dynamical system

$$\begin{aligned}
\frac{dx}{dt} &= \boldsymbol{H}_r \sin\theta\cos\varphi + \boldsymbol{H}_\theta \cos\theta\cos\varphi - \boldsymbol{H}_\varphi \sin\varphi\,,\\
\frac{dy}{dt} &= \boldsymbol{H}_r \sin\theta\sin\varphi + \boldsymbol{H}_\theta \cos\theta\sin\varphi + \boldsymbol{H}_\varphi \cos\varphi\,,\\
\frac{dz}{dt} &= \boldsymbol{H}_r \cos\theta - \boldsymbol{H}_\theta \sin\theta\,,
\end{aligned} \tag{30}$$

where x, y, z are Cartesian coordinates and t is a parameter; in the case of a Beltrami flow, t is just the time.

Our numerical integration scheme is the usual Runge-Kutta method in double precision, and typically Δt is taken as 0.2.

The configurations of the force-free magnetic field in the case $\ell = 1$ are regular. The lines of force always wind on some tori, the symmetric axis of which is the diameter connecting two nodes on the sphere. Figure 5 shows a stereoplot of such a torus corresponding to the superposition of the solutions $\ell = 1$, $m = 0$, and $\ell = 1$, $m = 1$ (the latter multiplied by 0.1).

Figure 6 shows the Poincaré sections of the line of force for the cases $m = 0$, $\ell = 2, 3, 4$. Since there exists a first integral in each case, all lines of force lie on ℓ families of tori, which are axisymmetrical with resepct to the polar axis. The center-lines of the tori are periodic orbits and are fixed points in the Poincaré section. The lines of force rounds the center-line with frequency ω_1, and at the same time gyrates about the z-axis with frequency ω_2. The ratio $n = \omega_1/\omega_2$ is called winding number. If the winding number is irrational, the orbit can cover an entire torus and the motion is quasi-periodic. The quasi-periodic orbits can be disrupted by certain nonlinear perturbations. If the winding number is rational, the orbit will eventually close on a torus, and the motion is periodic (resonance). Such a line of force is self-knotted and is known as a torus knot. The periodic orbit can break up into disjunct elliptic and hyperbolic orbits under small perturbations. Resonances will be discussed in the next section.

Figure 7 shows Poincaré sections corresponding to the situation that the integrable cases undergo small perturbations (taking the solutions of the same ℓ with $m \neq 0$ as perturbation terms). Most of the above ℓ families of tori still exist but undergo a slight distortion. These tori are known as KAM surfaces. Near the heteroclinic cycles of the integrable cases there is a chaotic layer. Under perturbations the stable and unstable manifolds may wrap in a very complicated way, so that their intersections may form a complicated web. All scattered points on each section of Fig. 7 correspond to a single line of force, for which 5000 successive intersections have been computed.

If we increase the strength of the perturbation, the chaotic layer will enlarge, and the regular region will decrease. In a strong mixture of the solutions of the same ℓ, a chaotic line of force may fill most of the sphere. Figure 8 corresponds to the superposition of the solutions $\ell = 3$, $m = 0, 1, 2, 3$. The chaotic region

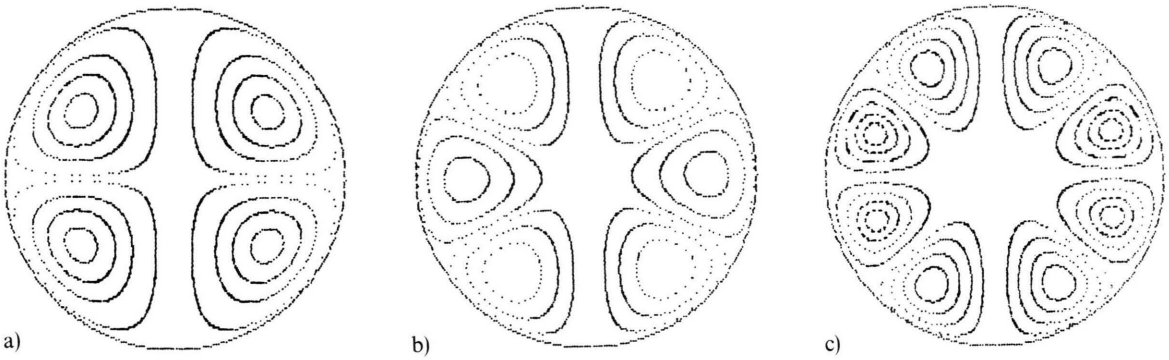

Fig. 6. Poincaré sections $x = 0$ for the case $m = 0$.
a) $\ell = 2$; b) $\ell = 3$; c) $\ell = 4$.

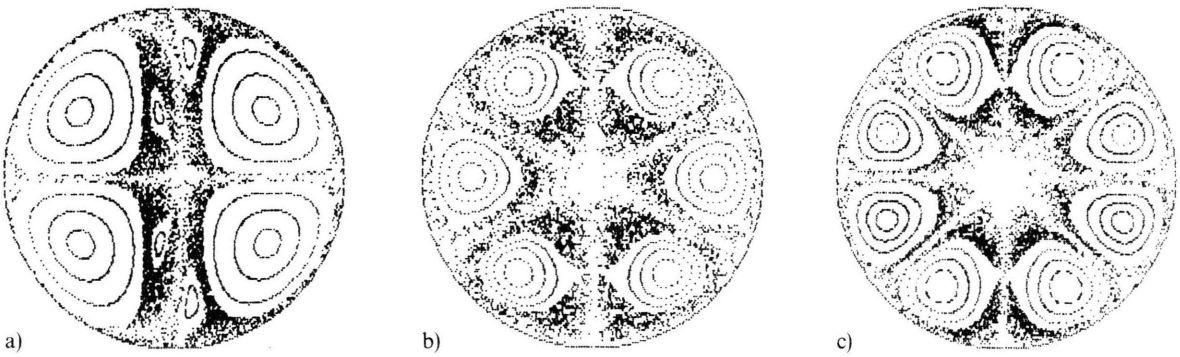

Fig. 7. Poincaré sections $x = 0$ corresponding to the situation that the integrable cases undergo small perturbations.
a) $\ell = 2$; b) $\ell = 3$; c) $\ell = 4$.

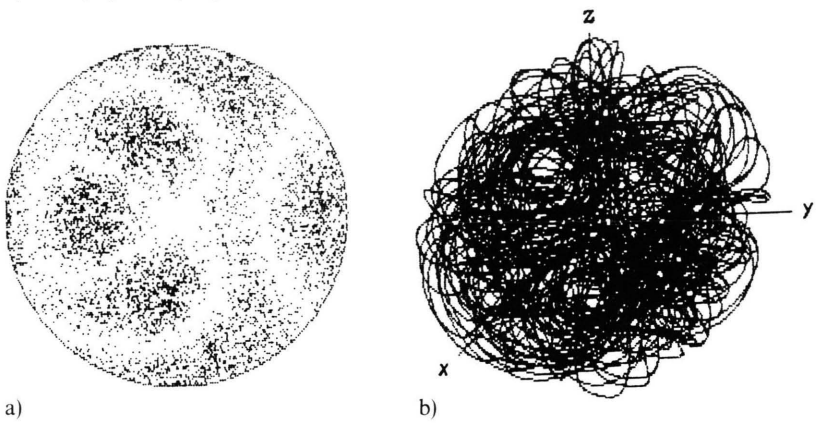

Fig. 8. A strong mixture of the cases $\ell = 3$; $m = 0, 1, 2, 3$.
a) Poincaré section $x = 0$.
b) Stereoplot of a chaotic line of force.

occupies a large fraction of the 3-D space in a sphere. A total of 5000 points, corresponding to a single line of force, are represented in Figure 8 a. Figure 8 b shows a stereoplot of a chaotic line of force corresponding to the same case.

The single solution, except the cases $m = 0$, seems to show a weakly chaotic behavior, but the superpositions of these solutions can cause conspicuous chaotic motion.

There exist complex topological structures in these force-free fields. For instance, Fig. 9 shows a tangled structure of two families or tori, which wind around each other three times and are surrounded and separated by a chaotic layer. This case corresponds to the

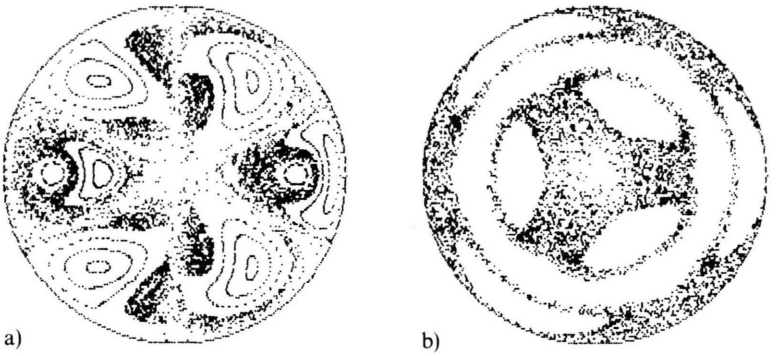

Fig. 9. Superposition of the cases $\ell = 3$; $m = 0$, and $m = 3$.
a) Poincaré section $x = 0$.
b) Poincaré section $z = 0$, the tangled structure of the regular regions imbeding in the chaotic layer.

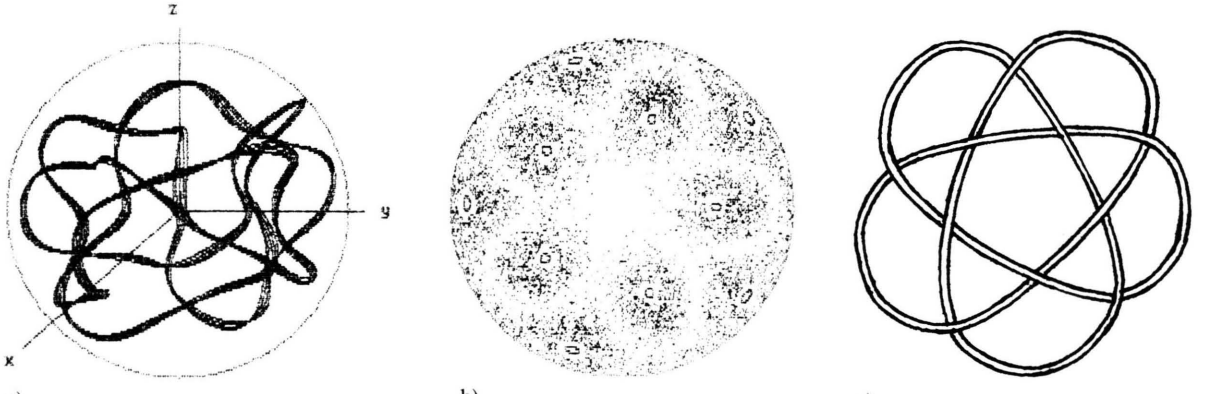

Fig. 10. Superposition of the cases $\ell = 5$; $m = 0$, and $m = 5$. a) Stereoplot of a complex self-knotted tube of force. b) Poincaré section $z = 0$. c) A knot of ten crossings.

superposition of the solution $\ell = 3$, $m = 0$, and $\ell = 3$, $m = 3$, (the latter multiplied by 0.1). The empty regions in Fig. 9 b are regular and occupied by quasi-periodic lines of force. There is a family of complicated self-knotted tori in the superposition case of the solutions $\ell = 5$, $m = 0$, and $\ell = 5$, $m = 5$, (the latter multiplied by 0.1). Figure 10 shows one self-knotted torus of such a family, which intersects the equator plane at ten closed curves (Figure 10 b). They are surrounded with scattered points produced by a single chaotic line of force. Such a self-knotted tube of force is topologically equivalent to a knot of ten crossings (Figure 10 c).

5. Resonances

Resonances are important in nonlinear dynamics, and often chaotic phenomena are associated with them. Through resonances the KAM surfaces can be disrupted, leading to increased chaotic regions. In order to show the resonances most clearly, we take a superposition of the solutions $\ell = 1$, $m = 0$; $\ell = 3$, $m = 0$; and $\ell = 3$, $m = 2$:

$$H = A(\text{Sol.}\,\ell = 1, m = 0) + B(\text{Sol.}\,\ell = 3, m = 0) + C(\text{Sol.}\,\ell = 3, m = 2), \quad (31)$$

where A, B, C are arbitrary constants.

The superpositions of the solutions which belong to the class of $m = 0$ produce regular configurations of the lines of force, since there still exists a first integral. Figure 11 a shows a Poincaré section of one family of tori, and which belongs to the case $A = 1$, $B = 0.4$, $C = 0$. A line of force rounds the center-line of the family of tori, at the same time gyrates about the polar axis. If the winding number is rational, the motion is periodic; if irrational, then quasi-periodic. Because the rational numbers are dense, there are infinitely many periodic orbits on a torus, and the classical analysis fails near the resonances.

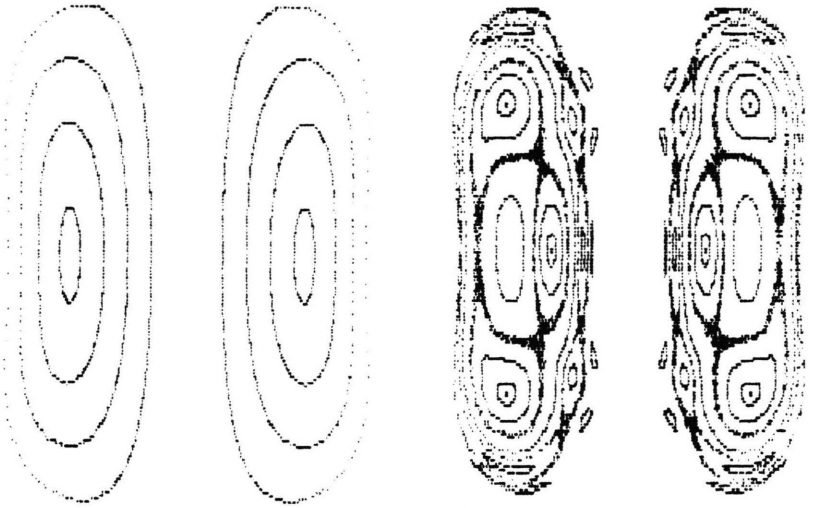

Fig. 11. Poincaré section $x = 0$ for the superposition of the cases $\ell = 1$ and $\ell = 3$.
a) Regular motion for the case $A = 1$, $B = 0.4$, $C = 0.0$.
b) Resonances and stochastic layers for the case $A = 1$, $B = 0.4$, $C = 0.0033$.

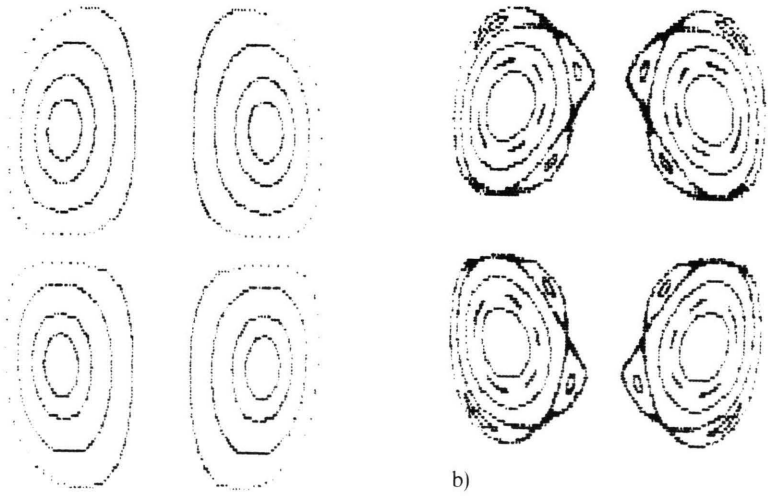

Fig. 12. Poincaré section $x = 0$ for the superposition of the cases $\ell = 2$ and $\ell = 4$.
a) Regular motion for the case $A = 1$, $B = 0.6$, $C = 0$.
b) Resonances for the case $A = 1$, $B = 0.6$, $C = 0.025$.

In order to show the strongest resonances, such as the 3:1 resonance, we superpose the solutions $\ell = 1$, $m = 0$, and $\ell = 3$, $m = 0$, so that the winding numbers could be adjusted by the coefficients A and B. Then, the solution $\ell = 3$, $m = 2$ serves as a perturbation term, and the coefficient C serves as a perturbation parameter. Figure 11 b is a Poincaré section for the case $A = 1$, $B = 0.4$, $C = 0.0033$, which shows the richest resonance behavior. In the inner region, KAM surfaces have been disrupted by the most conspicuous 3:1 resonance, and replaced by three families of islands, which are separated and surrounded by a marked stochastic layer. Near it, there is a chain of five small islands separated and surrounded by a thin stochastic layer. This is the 5:1 resonance, separated from 3:1 resonance by an intact KAM torus. In the outer region, there is a chain of seven islands. This is the 7:1 resonance, certainly surrounded by a thinner stochastic layer, which does not show in the figure, lest it becomes too complex to see.

Similarly, we superpose the solutions $\ell = 2$, $m = 0$; $\ell = 4$, $m = 0$; and $\ell = 2$, $m = 2$:

$$H = A(\text{Sol.}\,\ell = 2, m = 0) + B(\text{Sol.}\,\ell = 4, m = 0) + C(\text{Sol.}\,\ell = 2, m = 2), \quad (32)$$

where A, B, C are arbitrary constants.

First, we let $C = 0$. Under this condition, the line of force winds on a torus, and we can adjust the winding number by varying the coefficients A and B. Figure 12a shows a Poincaré section of two families of tori for the case $A = 1$, $B = 0.6$, and $C = 0$. Then, the solution $\ell = 2$, $m = 2$ is added as a perturbation term, which causes some periodic orbits to break up. Figure 12b is a Poincaré section for the case $A = 1$, $B = 0.6$, and $C = 0.025$. In the outer region there is a three-island chain surrounded by a thin stochastic layer; this is the 3:1 resonance; in the inner region, there emerges a chain of five small islands separated from the 3:1 resonance by some KAM tori. This is the 5:1 resonances.

6. Estimation of Dimension and Lyapunov Exponent

We now turn to investigate the quantitative characteristics of the dynamical behaviors. The dimension furnishes an estimate of the smallest number of the variables required to describe the system. The Lyapunov exponent is the average exponential rate of divergence or convergence of nearby orbits in phase space.

We estimate the correlation dimension D_2 using the method proposed by Grassberger and Procaccia [11], and estimate the largest Lyapunov exponent λ_1 using the method proposed by Wolf et al. [12]. These methods are based on a reconstructed pseudo phase space from a time series. We take the superposition of the solutions $\ell = 2$, $m = 0, 1, 2$:

$$H = A(\text{Sol.}\,\ell = 2, m = 0) + B(\text{Sol.}\,\ell = 2, m = 1) + C(\text{Sol.}\,\ell = 2, m = 2), \quad (33)$$

where A, B, C are arbitrary constants. The x-component of a line of force is taken to create a time series which consisted of 2048 points, separated by $\Delta t = 4 \times 0.2$. The time delay is $\tau = 4$.

In order to test the accuracy, we first use these methods to a periodic orbit, which is a center-line of one family of tori in the case $A = 1$, $B = C = 0$. The initial condition is $x = 0$, $y = 3.16003$, $z = 2.23448$. The result is: $D_2 = 1.03$, $\lambda_1 = 0.003$. This illustrates possible computational errors (the accurate values are: $D_2 = 1$, $\lambda_1 = 0$).

In the weakly perturbed case $A = 1$, $B = 0$, $C = 0.2$, the result for the line of force corresponding to the initial condition: $x = 0$, $y = 0.2$, $z = 4$, is $D_2 = 2.14$, $\lambda_1 = 0.028$.

In a strong mixture $A = B = C = 1$, the result for the line of force corresponding to the initial condition: $x = y = z = 1$, is $D_2 = 2.66$, $\lambda_1 = 0.035$.

A positive Lyapunov exponent characterizes the asymptotic orbital instability in phase space. This is an important feature of a chaotic orbit. According to Grassberger and Procaccia [11], we have

$$D_2 \leq D_1 \leq D_0, \quad (34)$$

where D_0 is the Hausdorff dimension and D_1 the information dimension. In the above case ($D_2 = 2.14$ or $D_2 = 2.66$), from (34), the Hausdorff dimension of a corresponding line of force is larger than its topological dimension $D_t = 1$. We thus truly get a fractal (Mandelbrot [13]).

[1] R. Lüst and A. Schlüter, Z. Astrophys. **34,** 263 (1954).
[2] L. Woltjer, Proc. Nat. Acad. Sci. USA **44,** 489 (1958).
[3] H. K. Moffatt, J. Fluid Mech. **35,** 117 (1969).
[4] V. I. Arnold, C. R. Acad. Sci. Paris **261,** 17 (1965).
[5] T. Dombre, U. Frisch, J. M. Greene, M. Hénon, A. Mehr, and A. M. Soward, J. Fluid Mech. **167,** 353 (1986).
[6] S. Chandrasekhar, Proc. Nat. Acad. Sci. USA **42,** 1 (1956).
[7] M. N. Rosenbluth and M. N. Bussac, Nuclear Fusion **19,** 489 (1979).
[8] E. A. Jackson, Perspective of Nonlinear Dynamics, Vol. **I,** Cambridge Univ. Press 1989, p. 248.
[9] I. Stewart, Does God Play Dice? Basil Blackwell, 1989, p. 108.
[10] Z. Y. Li and M. Qian, Theories and Applications on Rotation Degree of a Vector Field, Peking Univ. Press 1982.
[11] P. Grassberger and I. Procaccia, Phys. Rev. Lett. **50,** 346 (1983).
[12] A. Wolf, J. B. Swift, H. L. Swinney, and J. A. Vastano, Physica **16 D,** 285 (1985).
[13] B. B. Mandelbrot, The Fractal Geometry of Nature, Freeman 1977.